Advancements in americium-based ceramics for Radioisotope Power Systems
Material selection, fabrication and thermoelectric effect demonstration

Vigier, Jean François; Freis, Daniel; Konings, Rudy J.M.; Manaud, Jérémie; Raison, Philippe E.; Lajarge, Patrick; Gardeur, Sebastien; Vălu, Sorin Octavian; Griveau, Jean Christophe; More Authors

DOI
10.1016/j.mtchem.2025.103148

Publication date
2025

Document Version
Final published version

Published in
Materials Today Chemistry

Materials Today Chemistry 50 (2025) 103148

Contents lists available at ScienceDirect

Materials Today Chemistry

journal homepage: www.journals.elsevier.com/materials-today-chemistry/

Advancements in americium-based ceramics for Radioisotope Power Systems: Material selection, fabrication and thermoelectric effect demonstration

Jean-François Vigier [a], Daniel Freis [a], Rudy J.M. Konings [a,b], Jérémie Manaud [a], Philippe E. Raison [a], Patrick Lajarge [a], Sebastien Gardeur [a], Sorin Octavian Vălu [a], Jean-Christophe Griveau [a], Karin Popa [a,*]

[a] European Commission, Joint Research Centre (JRC), Karlsruhe, Germany
[b] Faculty of Applied Sciences, Radiation Science & Technology Department, Delft University of Technology, Mekelweg 15, Delft, 2629JB, the Netherlands

ARTICLE INFO

Keywords:
Actinide
Ceramic
Nuclear materials
Radiation effects
Thermoelectricity

ABSTRACT

This work provides an in-depth analysis of the extensive research and development activities on americium-based ceramics for space applications, particularly as heat source for radioisotope power generation. Our pioneering efforts focus on synthesizing and characterizing various americium ceramics with fluorite, monazite, perovskite, zircon, and pyrochlore structures, and assessing their potential for use in Radioisotope Power Systems (RPSs). This study identifies uranium-stabilised cubic americium oxide as the best candidate among the ceramic forms analysed, due to its superior stability and performance under extreme conditions relevant to space missions. The review emphasises the unique facilities and methodologies employed, including remote-handling techniques and advanced material characterization, to overcome the challenges posed by the high radiation dose and specific activity of ^{241}Am when working with gram quantities.

1. Introduction

The main methods of generating heat and power for space missions are nowadays based on photovoltaics and chemical energy generation [1,2]. For long-term missions into the outer regions of the solar systems or exploration of planetary bodies with long nights, sun-independent power systems such as Radioisotope Heater Units (RHU) and Radioisotope Thermoelectric Generators (RTGs) are used, which are powered by the decay heat of radioactive isotopes. Heat is then used for temperature control or is converted into electricity by thermoelectric conversion [3]. The selection of suitable radioisotopes and their chemical and physical form as heat source material for Radioisotope Power Systems (RPSs) is based on a long list of criteria [4]. These include half-life long enough but high isotopic power, and low levels of radiation. The matrix should present high power density, be chemically stable and serve as a stable host for decay products, be compatible with encapsulation materials and with the operating and post-accident environments and be resistant to extreme conditions. It should also not disperse into inhalable small particles, have low solubility in the environment and the human body, among others.

With a few exceptions where ^{210}Po was employed, all RHUs and RTGs for space exploration have used ^{238}Pu as fuel, producing 0.57 W g^{-1}, in its oxide form (PuO_2). The most well-known example is the case of the two Voyager interplanetary probes, which are equipped with RTGs providing hundreds of watts of power at the time of their launch using SiGe thermoelectric convertors as well as a number of RHUs [5,6]. However, due to the limited stock of ^{238}Pu and the challenges in obtaining this radioisotope [7], alternatives such as ^{241}Am that can be extracted from stockpiles of reprocessed plutonium, are becoming increasingly attractive.

The americium isotope ^{241}Am is formed *via* β^--decay of ^{241}Pu (which has a half-life of 14.33 years). Due to its accumulation in existing stocks of civil separated plutonium in Europe, and its relatively high specific power of 0.114 W g^{-1}, ^{241}Am (half-life of 432.2 years) [8] is under consideration by the European Space Agency (ESA) as a power source for future European space missions [9]. Americium (^{241}Am and ^{243}Am) is one of the main contributors to the long-term radiotoxicity of civil nuclear waste (after plutonium) and its separation and re-use will reduce

* Corresponding author.
E-mail address: karin.popa@ec.europa.eu (K. Popa).

https://doi.org/10.1016/j.mtchem.2025.103148
Received 7 July 2025; Received in revised form 23 September 2025; Accepted 20 October 2025
Available online 29 October 2025

the potential impact of geological storage [10]. Thus, as part of an existing circular process, this approach utilises a cheaper and relatively abundant by-product of nuclear reactors that would otherwise not have obvious use [11,12]. In recent decades, significant amounts of ^{241}Am have been extracted from reprocessed plutonium at the Sellafield reprocessing plant in the UK [13] and La Hague in France. Application for RPSs would thus be quite useful as it gives an opportunity to use, at least partially, ^{241}Am generated in nuclear fuels used for civil electricity production. The potential use of ^{242m1}Am (half-life of 141 years) in space applications was also under consideration [14]. However, this isotope is easily fissioned during reactor operation and thus found in minimal quantities in the nuclear waste. It can be produced by the irradiation of ^{241}Am with thermal neutrons, and separation from the parent ^{241}Am can only occur through electromagnetic methods [15]. Very recently, preliminary information has appeared regarding the use of ^{243}Am (half-life of 7370 years) in micronuclear batteries for very low-power applications [16].

In this context, ESA has initiated the EuropeaN Devices Using Radioisotope Energy (ENDURE) program for developing long-lasting heat and electricity units powered by americium for upcoming ESA Moon missions in the next decade [17]. Within a Collaborative Research Agreement between ESA and its subcontractors and the Joint Research Centre (JRC), a chemically stable fuel material for ^{241}Am based RPSs has been investigated [18]. In parallel, our group produced and studied several ceramic forms containing significant specific Am-amounts. While previous reports focussed on individual americium compounds, this work represents the first systematic head-to-head comparison of multiple americium ceramic families (oxides, phosphates, aluminates, vanadates, zirconates) synthesised and evaluated under a unified experimental framework. This integrative approach provides a transparent, criteria-based selection process, which has not been attempted in earlier works.

2. Candidate ceramic materials

The metallic form is the material with the highest ^{241}Am content, thus a specific power of 0.114 W g^{-1}. However, high chemical reactivity, low thermal stability and reduced stability under α-irradiation of metallic americium [19] are not favourable for RPS's.

The next class of compounds in term of specific power density would be the binary oxides (AmO_2 and Am_2O_3). Note that americium-oxygen system shows complex behaviour [20,21]. Cubic dioxide (AmO_2) loses oxygen at high temperatures and in vacuum, with increase in volume and conversion into hexagonal sesquioxide (Am_2O_3). In turn, Am_2O_3 is prone to oxidation and converts into AmO_2 in air (even at room temperature). In both cases dimensional changes can cause disintegration of pellet. Their stability in vacuum, oxidising and reducing conditions is discussed by Vigier et al. [22], who concluded that americium dioxide can be stabilised by insertion of uranium, leading to the cubic An_2O_{3+x} C-type oxide (fluorite-related structure).

Another option would be the use of a ternary ceramic oxide, although incorporation of other elements will further decrease the Am-content and specific power. Thus, compounds containing light(er) elements would be preferable, but many light elements are prone to *(α,n)* nuclear reactions, increasing the neutron production of the source. This makes, for example, materials based on lithium, boron or beryllium highly irrelevant for this application [23]. In oxide ceramics, such *(α,n)* reactions occur for ^{17}O and ^{18}O having a natural abundance of 0.04 % and 0.20 % respectively, while they do not occur for ^{16}O (99.76 %) [24]. Therefore, the neutron production of the materials in the source must be reduced by using oxygen depleted in ^{17}O and ^{18}O.

In September 2025, the Inorganic Crystal Structure Database (ICSD) [25] summarized about 150 reports on crystalline (experimental inorganic and metal-organic) structures containing americium (Fig. 1), one-third refers to oxygen-containing compounds. More structures and references to Am-inorganic and organic compounds are listed in, *e.g.*,

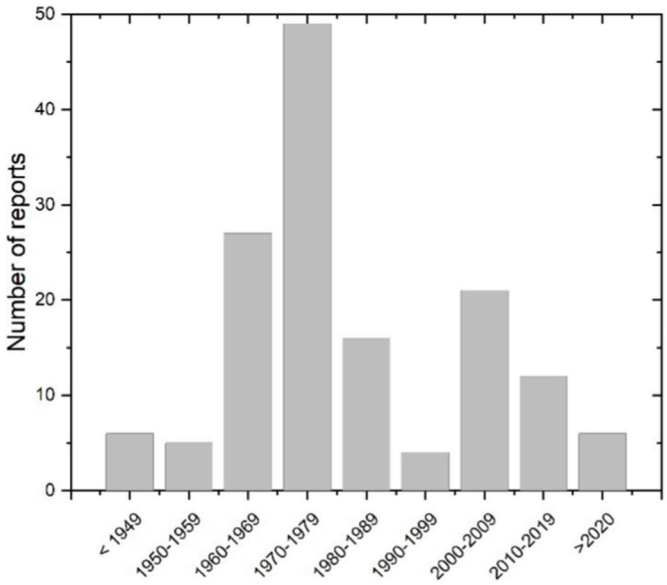

Fig. 1. Number of ICSD reports on americium compounds per decade, highlighting the lack of crystallographic studies on this element. Most of the reports are from the decade 1970–1979, with renewed attention in the last two decades. Note that the isotopy of americium vector is not always revealed in these works [27]. The more stable ^{243}Am is currently used to a greater extent on the expenses of the ^{241}Am. While the first publications originate from the Los Alamos Nuclear Site, since the 1970s, many of them come also from the former Soviet Union and the Federal Republic of Germany.

"*Americium: Chemistry of Actinide and Transactinide Elements*" [26]. The low number of well characterised crystalline Am-compounds is in line not only with the restricted access to this element, but also with the limited stability under self-irradiation of the crystalline compounds. In the next section we will discuss those compounds that could be relevant as RTG source material.

3. Comparison of relevant ceramics

The following ceramic compounds of high Am-content are considered in our evaluation: $Am_{1-y}U_yO_{2-x}$ (fluorite-related structure), $AmPO_4$ (monazite-like), $AmAlO_3$ and $AmVO_3$ (perovskite-like), $AmVO_4$ (zircon-like), and $Am_2Zr_2O_7$ (pyrochlore structure). The main criteria ruling the initial selection of these compounds were: *(i)* existence of stable natural surrogates; *(ii)* reduced or moderate reactivity with relevant atmospheres (vacuum in space, air in re-entry accidents); *(iii)* presence of literature on radiation stability of the class of compounds. In addition, the distribution and possible segregation of the decay product ^{237}Np is an important criterion, because when segregated as a fluorite *fcc* secondary phase it creates interfaces and induces stress in the material. Furthermore, the large quantity of helium released should also be taken into account and the design of the encapsulation adapted accordingly. Finally, the thermal properties, and specifically the thermal conductivity, need to be considered, in view of thermal performance.

3.1. Structural features

The structures of americium compounds considered here are reported in Fig. 2.

They can be separated in three categories depending on their level of crystallographic compactness. The lowest level of compaction is observed for the oxyanionic compounds $AmPO_4$ (monazite-like, $P12_1/n1$) and $AmVO_4$ (zircon-like, $I4_1/amd$), consisting of a framework in which trivalent americium is linked by isolated tetrahedron units (PO_4^{3-} and VO_4^{3-}, respectively). Higher level of compaction is reached for

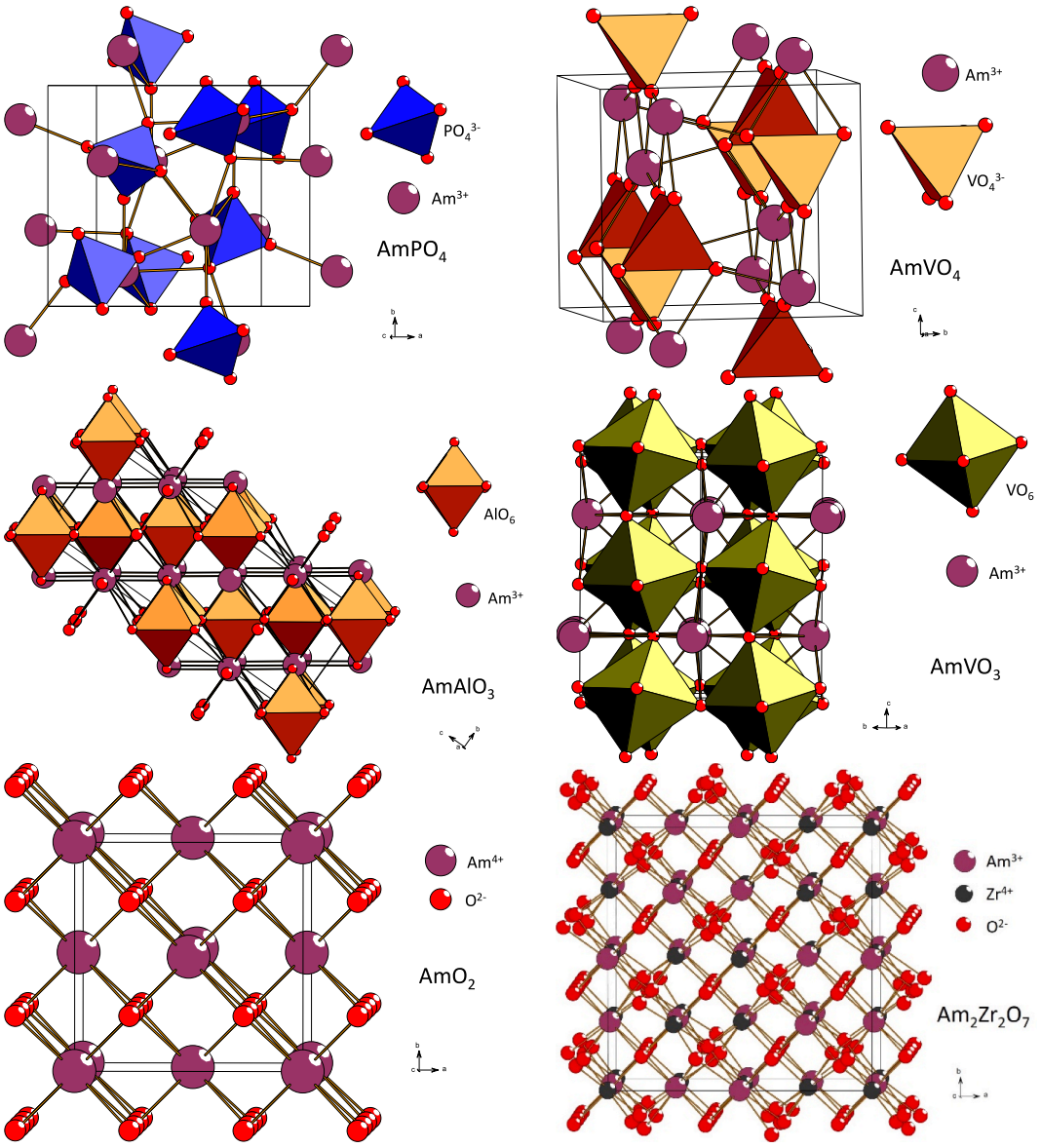

Fig. 2. Views of the structure of the different americium compounds under consideration. $AmPO_4$ has a $P12_1/n1$ (14) monazite type structure [28], $AmVO_4$ a $I4_1/amd$ (141) zircon-type structure [29], $AmAlO_3$ a R-3cH (167) perovskite structure [30], $AmVO_3$ a Pbnm (62) perovskite structure [29,31], AmO_2 a Fm-3m (225) fluorite structure [32], $Am_2Zr_2O_7$ a Fd-3m (227) pyrochlore structure.

americium compounds adopting close-packed perovskite configuration like $AmAlO_3$ and $AmVO_3$. Their structures consist of an arrangement of octahedron units linked to each other by their vertices and with americium cation in the middle. Like all the different variations of perovskite-based structures, $AmAlO_3$ (*R-3cH*) and $AmVO_3$ (*Pbnm*) can be derived from the basic regular cubic perovskite configuration (*Pm-3m*) with slight distortion and tilt of the octahedron units. Finally, the highest level of compaction is reached for the close-packed fluorite (AmO_2, *Fm-3m*) or fluorite-related compounds (like zirconate pyrochlore, $Am_2Zr_2O_7$, *Fd-3m*).

Thus, AmO_2 seems a logic choice, but it has a limited thermal stability, and tends to lose oxygen, as discussed by Vigier et al. [22]. These authors concluded that americium dioxide can be stabilised by insertion of uranium, resulting in a fluorite-related structure. As shown by Epifano et al. [33,34] mixed $(U,Am)O_2$ oxide with up to 67 % Am/(Am + U) content, produced by powder metallurgy [33,35,36], display a very rich level of cationic valences, with charge transfer leading to the presence of not only Am^{4+} and U^{4+} but also Am^{3+} and U^{5+}, making the interpretation of lattice parameters complex [37,38]. The uranium stabilised americium oxide for space applications in our work [22] differs from other uranium and americium mixed oxides reported in the literature due to its very high americium content ($Am/M = 80$ %), in particular its high lattice parameter shows a high level of reduction. Therefore, even if it is related to a substoichiometric fluorite dioxide $(U,Am)O_{2-x}$, it corresponds, from the crystallographic point of view, to hyper-stoichiometric C-type sesquioxide $(U,Am)_2O_{3+x}$, *i.e.* the stabilised form of the reported cubic C-type Am_2O_3 [20].

The fluorite and fluorite-related mixed oxide show a high-level of chemical flexibility, with a single cationic crystallographic position having the possibility to contain different actinides of different valence states, the overall charge of the oxide being compensated with oxygen ions vacancies or interstitials. $(U,Am)_3O_{2+x}$ is therefore a good host for ^{237}Np (daughter element) produced during α-decay of ^{241}Am and form a homogeneous mixed oxide [22]. It seems, from characterisation of synthesised $AmPO_4$ [28] and $AmVO_4$ [29], that these two structures have a very low level of segregated NpO_2 despite its presence at about 7 % Np in the americium source, indicating that these two compounds can host at least few percent of the daughter element. Finally, perovskites do

not seem to be a good host for neptunium, which clearly segregated during the synthesis of $AmAlO_3$ [30] and $AmVO_3$ [29].

In the Am_2O_3–ZrO_2 system, the specific composition with 50 % of americium and 50 % of zirconium cations become long-range ordered as shown in Fig. 2, adopting the so-called pyrochlore structure [39–41]. This structure, of general formula $A_2B_2O_7$, or more accurately $A_2B_2O_6O'$, is isometric (*Fd-3m*, Z = 8, *a* = 9–12 Å) and it can be commonly described as a fluorite-type with a double unit cell and an ordered deficiency of 1/8 of oxygen atoms (represented as a "" in the formula) [42–44]. The typical *A/B* radii ratio is between 1.46 and 1.80 [45], and the Am^{3+}/Zr^{4+} value fits well in this range. Due to the relatively high actinide content of $Am_2Zr_2O_7$, and its good radiation resistance (see below), it appears reasonable that $^{241}Am_2Zr_2O_7$ could be an interesting source material for RPSs for space applications.

3.2. Radiation stability

In our studies, the synthesis of all the compounds was targeted to produce 100 mg of the final product (specific activities in the range of 10^{10} Bq), except for the U-stabilised AmO_2, which was made on a larger scale of several grams (~10^{12} Bq).

Each α-decay of ^{241}Am emits a He-ion of 5.49 MeV energy which is stopped by electronic interactions over 10–20 μm, generating between 100 and 200 displacements along its trajectory. The decay also involves a recoil of the daughter ^{237}Np of 92 keV energy which is stopped by nuclear interactions over a much shorter distance (~20 nm) but associated with about 1500 displacements. The self-irradiation stability was determined by powder X-Ray Diffraction (XRD) analysis of the samples over prolonged periods (months to years). Approximately 10 mg of powder was immobilised in a bi-component epoxy resin on a sample holder for crystallographic analysis and stability studies. The material behaviour in this design may not perfectly mirror that of bulk materials in sintered pellets; however, it does offer a reasonable representation and allows for a meaningful comparison of the stability of each composition.

As shown in Fig. 3, the fluorite and fluorite-related compounds (zirconate pyrochlore and stabilised C-type $(U,Am)_2O_{3+x}$) show an excellent tolerance against α self-irradiation, the materials remaining crystalline and exhibiting a very moderate swelling (less than 1 % of the initial lattice volume). AmO_2 keeps its crystallinity up to at least 36 displacements per atom (dpa) [46]. $(U,Am)O_2$ of various compositions [47] shows very similar behaviour as pure AmO_2 with a crystallographic volume stabilisation at about 0.8 % of the initial volume. In contrast, uranium stabilised C-type $(U,Am)_2O_{3+x}$ shows a significantly lower swelling [22], which can be understood from its specific C-type configuration with a vacant site on the oxygen sublattice and a higher degree of disorder on the cation sublattice.

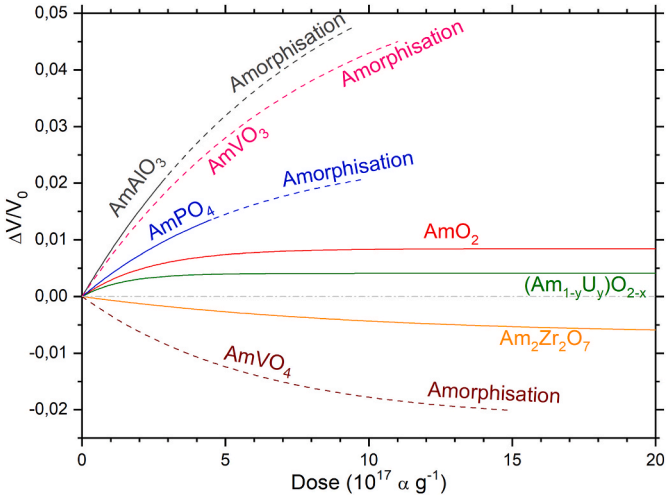

Fig. 3. Crystallographic lattice volume variation for different americium compounds (including AmO_2 [20] and $Am_2Zr_2O_7$ [48]. The solid lines are exponential fit of experimental values obtained from Rietveld refinement. Dashed lined are only estimation: for high dose $AmAlO_3$ and $AmPO_4$ shows important peak broadening and asymmetry preventing from accurate Rietveld refinement, while for $AmVO_3$ and $AmVO_4$ the volume variation was estimated from two Rietveld refinements only.

Natural monazite-(Ce) generally exhibits moderate resistance to radiation damage from α self-irradiation, attributed to continuous low-temperature annealing [49–51]. The damage is caused by α decay from uranium and thorium that substitute for Ce from a few percent to very high amounts (see *e.g.* Ref. [52]). As observed for $PuPO_4$ and $AmPO_4$, amorphization of monazite-type phases can occur at relatively low doses of self-irradiation, depending on the composition [53,54]. For example, ^{238}Pu-doped $(La,Pu)PO_4$ remained crystalline up to a higher cumulative dose than pure $PuPO_4$, which became almost completely amorphous. Increasing the Pu-content in monazite solid solutions diminishes its resistance to self-irradiation [55,56]. Americium phosphate, $AmPO_4$, remained crystalline under self-irradiation for circa two months, with a crystallographic volume swelling of ~1.5 %, and then was amorphising over a period of a year. However, microcrystals were present in the amorphous material even after a two-year period [28].

Zircon ($ZrSiO_4$) is frequently found in nature in the metamict (amorphous) state due to damage caused by α self-irradiation from incorporated uranium and thorium decay [57]. The accumulation of radiation damage in zircon is associated with changes in its physical properties and a general decrease in its chemical durability [58]. Research on natural zircon, ^{238}Pu-doped zircon, and ion-beam irradiated zircon has provided a clear understanding of radiation effects on zircon across different time scales [59]. Radiation damage causes the buildup of point defects and amorphous regions in zircon. Amorphous zircon recrystallises above 1000 °C in two steps, starting with formation of pseudo-cubic zirconia. As shown in Fig. 3, the zircon-type $AmVO_4$ shows a rapid amorphization, but with a lattice contraction, possibly due to a phase transformation [29].

The effect of americium α-decay on americium aluminate has been monitored by XRD and ^{27}Al Magic Angle Spinning – Nuclear Magnetic Resonance (MAS NMR) analyses. In a first step, a progressive increase in the level of disorder in the crystalline phase was detected, associated with a significant crystallographic swelling of the material. In a second step, the crystalline $AmAlO_3$ perovskite was progressively converted into amorphous $AmAlO_3$, with a total amorphization occurring after 8 months and $2{\cdot}10^{18}$ α-decays g^{-1}. The material showed a significant swelling (~5 % of the lattice volume) followed by total amorphization [30]. The trivalent oxidation state of americium was stabilised in the $AmAlO_3$ perovskite in oxidising conditions, which is beneficial for its use as an americium-bearing material. As a drawback, a clear segregation was observed of the ^{237}Np impurity initially present in the americium within the oxide phase. Moreover, the neutron yield from *(α,n)* in aluminium is not negligible for the α-decay energy of ^{241}Am [23,60].

Pyrochlore-like compounds are found in igneous rocks (such as carbonatites, nepheline syenites or granite pegmatites) containing up to 30 *wt*% UO_2 and 9 *wt*% ThO_2 [61]. Several studies on radiation resistance have been performed with actinide doping of zirconates. XRD measurements showed that $^{243}Am_2Zr_2O_7$ and $^{249}Cf_2Zr_2O_7$ both exhibits very good resistance to α self-irradiation [62]. The compound with californium, which has a shorter half-life, showed a slight swelling of the lattice parameter during the first months and lost progressively the characteristics diffraction lines belonging to the pyrochlore superstructure. After six months of self-irradiation (corresponding to $1.17{\cdot}10^{18}$ α-decay g^{-1}) the diffraction lines of the superstructure disappeared but the compound remained crystalline, transformed into disordered fluorite solid solution. Two years later the compound was still crystalised in a cubic solid solution. In a similar study [48] it was shown that the initial lattice parameter of $^{241}Am_2Zr_2O_7$ decreased by about 1 % after three

months. Furthermore, the superstructure peaks vanished slowly and completely disappeared after a year, corresponding to a cumulated dose of 0.21 dpa. The same study showed that the compound remained crystalline as a cubic solid solution after an experimental period of 1360 days, corresponding to a cumulated dose of 0.8 dpa. In case the actinide ions are oxidized to the tetravalent oxidation state, an order-disorder phase transition occurs, which is the case for the americium [63–65]. Accordingly, the compound $Am_2Zr_2O_7$ is only stable under inert atmosphere.

3.3. Helium release

Helium produced from alpha decay of ^{241}Am has an influence on the source material behaviour because it accumulates in the crystal structure and at the grain boundaries of the microstructure [66]. As a result, the physical and mechanical properties will evolve with time. From studies of helium in natural minerals containing uranium and thorium, as well as in nuclear fuel behaviour, the mechanisms underlying its behaviour are well known. Helium atoms are trapped in lattice defects, voids or pores, and then aggregate into gas bubbles in grains or at grain boundaries through lattice diffusion. With increasing time, and the concomitant increase of defects and He concentration, the bubbles will grow and aggregate further, particularly at grain boundaries. This leads to macroscopic swelling (in combination with the lattice swelling discussed in the previous section), cracking and fragilization of the pelletised material.

The behaviour of helium is known in some of the selected materials. The diffusion of radiogenic helium in zircon and monazite has been studied in natural materials [67,68], in which He generating radionuclides (Th, U) have a much lower concentration and He generation rates than pure americium compounds. The diffusion coefficients of ion-implanted helium in monazite and zircon were found to be close in the temperature range 575 K–873 K [69,70]. An interesting observation of these studies was that He diffusivity in synthetic $LaPO_4$ was about an order of magnitude faster than in natural monazites. This can be related to the trapping effect at defects created by self-irradiation and substitutional impurities. Studies on helium behaviour in pyrochlore ($Gd_2Zr_2O_7$) show a similar effect [71]. Extensive literature exists on the helium behaviour in fluorite structure actinide dioxides (*e.g.* Refs. [72–74]). Helium release takes place at temperatures between 500 K and 1400 K (with peak at 1200 K) when samples are heated in a continues manner. It follows the stages described in the previous paragraph, with the peak release corresponding to the grain boundary opening and release. Also, for fluorite, the defect structure as well of the oxygen-to-metal ratio (O/*M*) of the material play an important role. Because RHUs and RTGs sources operate in this temperature range, helium diffusion takes place, and the release can be tuned by engineering the microstructure for the pelletised material. An open porosity structure must be aimed at to facilitate release, as is the case for $^{238}PuO_2$ sources [75] optimised with respect to density and mechanical stability. Helium release is thus only partially a material intrinsic characteristic and therefore is scored "zero" the performance assessment.

3.4. Thermal properties

Thermal properties of the selected americium compounds are poorly known [76]. While structure and radiation effects can be studied on small-scale samples as described in the previous sections, thermal property studies need large(r) quantities that are generally not available, except for the binary oxide. Therefore, the thermal properties must be assessed from lanthanide surrogates in most cases. In our work we have focussed on the thermal conductivity. This property is highly sensitive to self-irradiation effects [74,77], and thus will change rapidly from the moment of fabrication of the source [78–80] so already well before employment in space.

At room temperature a significant difference exists for the thermal conductivity of the compounds, with the close-packed pyrochlore at the lowest range (1.3 W m^{-1} K^{-1}) [81], fluorite and monazite at intermediate (2.5–3 W m^{-1} K^{-1}) [82,83] and zircon and perovskite at the high range (>7.5 W m^{-1} K^{-1}) [84,85]. At higher temperature, these differences disappear, and the available data show thermal conductivities in the range of 1–2 W m^{-1} K^{-1}. The radiation damage created by the alpha decay of ^{241}Am will rapidly lead to further reduction, as has been evidenced by heat capacity [78] and thermal diffusivity measurements [74]. Thus, we expect the differences between the materials to be small under operating conditions in space.

3.5. Performance evaluation

Based on this extended discussion, the selected criteria and scores used for the assessment of the ceramics under consideration are shown in Table 1. The limits for this comparison were defined based on the current knowledge, realising that due to radiological safety limitations, americium ceramics can only be prepared in the milligram-to-gram range. When synthesis scale will become larger in the future, the criteria and scores be can adjusted further based on new findings. The individual performances of the selected ceramics, for ten essential criteria, are summarized in Table 2. Note that some information related to the thermal stability under different atmospheric conditions is missing and not considered in the final assessment (no score) in Table 3. This comparative clearly shows that, among the selected compounds, the fluorite related $Am_{1-y}U_yO_{2-x}$ is the most suitable ceramic for use in RPSs.

4. Am-ceramics fabrication

The fabrication of Am-ceramics is complicated by the high specific activity of ^{241}Am (126.91 GBq g^{-1}) and the fact that the α-decay of ^{241}Am is accompanied by a γ-emission of 59.5 keV. As a result, the traditional way of handling actinides, alpha-tight glove boxes, is only suited for small quantities in the order of a few milligrams. The solution to this is shielding and remote handling. Shielding of glove boxes with lead glass will help to limit the body dose, but not the dose on the hands; lead shielded gloves complicate the work significantly. These measures will only lead to a small increase of the quantities that can be handled. Therefore, remote handling and robotisation are the ultimate solution for the handling of larger ^{241}Am quantities, which are required for RPSs.

The JRC-KA site of the European Commission (EC) [86] has operated such remote facilities for many decades, being one of the few facilities dedicated to the fabrication of materials containing minor actinides (MA) in the European Union (EU). A laboratory in operation since 2004, the so-called Minor Actinide Laboratory (MALab), is primary dedicated

Table 1
Criteria defined for the assessment of suitability of specific ceramic for use in space missions.

Criteria		Score		
		−1	0	1
Power density at 100 % TD (W cm^{-3})		<75	75–85	>85
Volume variation δ (%)		δ < −2 or δ > 2	(-2 < δ < −1) or (1 < δ < 2)	(-1< δ < 1)
Amorphization		fast	slow	no
Stability	oxidising	RT – 500 °C	500°C–1000 °C	>1000 °C
	inert	RT – 500 °C	500°C–1000 °C	>1000 °C
	reducing	RT – 500 °C	500°C–1000 °C	>1000 °C
^{237}Np-distribution		segregation	segregation + atomic scale	atomic scale
(α,n) reaction with associated cation		yes		no
Helium release		large effect	mild effect	no effect
Thermal conductivity at RT, W m^{-1} K^{-1}		<2	2–5	>5

Table 2
Assessment of the individual performances of the selected ceramics based on the defined criteria. To facilitate comparisons with other materials, the power density is also provided in W g^{-1}.

Ceramic		$AmVO_3$	$AmVO_4$	$Am_{1-y}U_yO_{2-x}$	$AmPO_4$	$AmAlO_3$	$Am_2Zr_2O_7$
Structure		perovskite	zircon	fluorite related	monazite	perovskite	pyrochlore
Power density at 100 % TD (W cm^{-3})		0.77	0.53	0.88[a]	0.62	0.86	0.60
Power density (W g^{-1})		0.081	0.077	0.082[a]	0.082	0.087	0.071
Volume variation δ (%)		+4.2	−1.8	+0.4	+1.5	+5	−0.6
Amorphization		fast	fast	no	slow	fast	no[c]
Stability	oxidising	RT–280 °C	RT–1500 °C	<200 °C [b]	RT–1500 °C	RT–1500 °C	([d])
	inert				RT–1500°C		
	reducing	RT–1250 °C		RT–1600 °C		RT–1400 °C	RT-1400 °C
^{237}Np-distribution		segregation	atomic scale + segregation	atomic scale	atomic scale + segregation	segregation	
(α,n) reaction with associated cation		no	no	no	no	yes	no
Helium release		mild effect	mild effect	mild effect	mild effect	mild effect	mild effect
Thermal conductivity at RT, W m^{-1} K^{-1}		>7.5	>7.5	2.5–3	2.5–3	>7.5	1.3

[a] Can be improved by the optimisation of the Am/(Am + U)-ratio.
[b] This material oxidises between 100 and 200°C, but the structure stays the same and behaves well during oxidation.
[c] Phase transition from pyrochlore to defect-fluorite structure observed after a self-irradiation to a dose of 0.21 dpa.
[d] It oxidized into fluorite structure [41], but the temperature is not reported.

Table 3
Score attribution based on the assessment of the individual performances of the selected ceramics.

Ceramic		$AmVO_3$	$AmVO_4$	$Am_{1-y}U_yO_{2-x}$	$AmPO_4$	$AmAlO_3$	$Am_2Zr_2O_7$
Structure		perovskite	zircon	fluorite related	Monazite	perovskite	pyrochlore
Power density at 100 % TD (W cm^{-3})		0	−1	+1	0	+1	−1
Volume variation δ (%)		−1	0	+1	0	−1	+1
Amorphization		−1	−1	+1	0	−1	+1
Stability	oxidising	−1	+1	−1	+1	+1	
	inert				+1		
	reducing	+1	−1	+1		+1	+1
^{237}Np-distribution		−1	0	+1	0	−1	
(α,n) reaction with associated cation		+1	+1	+1	+1	−1	+1
Helium release		0	0	0	0	0	0
Thermal conductivity at RT, W m^{-1} K^{-1}		+1	+1	0	0	+1	−1
Score		−1	0	+5	+3	0	+2

to fabricating materials containing minor actinides such as americium and curium. It does not consist of classical hot cells, but rather of remotely operated gloveboxes behind thick radioprotection walls. The protection is composed of two layers: *(i)* lead bricks of 5 cm and windows with equivalent shielding of the γ-radiation, *(ii)* shielding of neutrons from spontaneous fission by polyethylene and water, 50 cm at the working level and 10 cm to shield against stray radiation (Fig. 4a). The protection walls are movable so that manual maintenance of the glove boxes and equipment therein is possible once the radioactive sources have been moved to storage positions with the same shielding equivalent.

The maximum mass of ^{241}Am that can be handled in the MALab is 50 g, which is not determined by the thickness of the shielding but is the result of the safety cases in the license. The quantities for ^{242m1}Am and ^{243}Am are 0.1 g and 65 g, respectively. In fact, the thickness of the lead shielding is chosen for the handling of ^{231}Pa (maximum 10 g) and that of

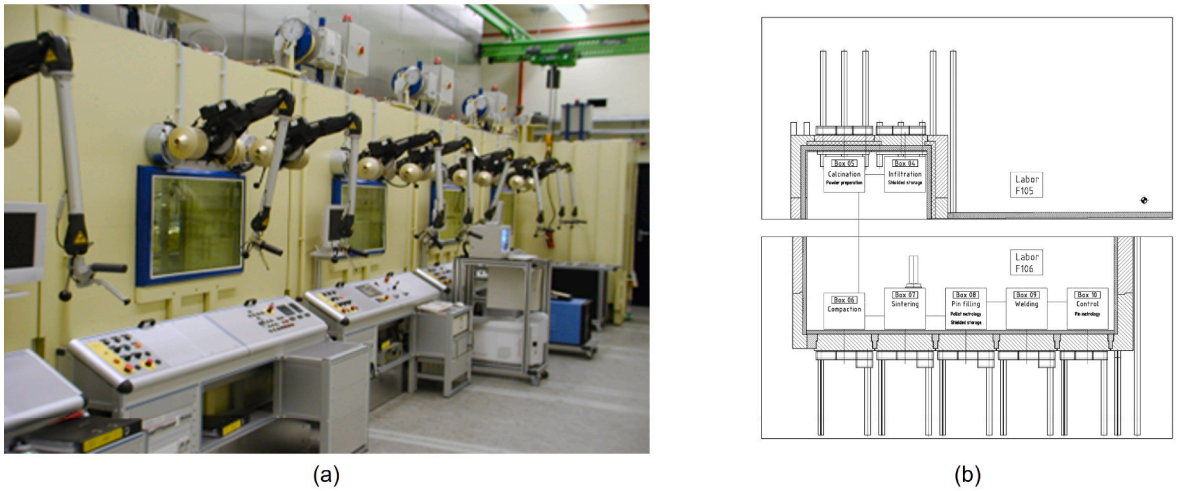

(a) (b)

Fig. 4. (a) The Minor Actinide laboratory at JRC-KA showing the shielded of glove boxes at the working level (yellow), the manipulators for remote handling, and the metal encased shielding for the stray radiation (top). Note that the side wall in the back is opened. (b) Schematic layout of the MALab at the JRC-KA showing the remotely operated seven glove boxes and their function behind the radioprotection for γ- and neutron radiation.

the neutron shielding for ^{244}Cm (maximum 5 g), based on the JRC-KA *in-house* dose limits for workers.

This hybrid concept of heavily shielded and remotely operated glove boxes requires that background radiation levels in the glove boxes remains low and for that reason fabrication processes should be nearly dust-free. Wet chemistry (sol-gel, precipitation, hydro-/solvothermal) or infiltration methods are well implemented, whereas dry chemistry (powder mixing) is only used for a restricted number of steps for the pellet preparation. The seven cells of the MALab (see Fig. 4b) comprise all key processes for the fabrication such as mixing/blending, calcination, pressing, sintering (in different atmospheres), plus the basic characterisation of the aspect and dimensions of the fabricated ceramics.

Several Am-ceramics have been synthesised and handled over the past decades for various purposes. These include fuels for transmutation comprising inert matrix fuels, ceramic waste forms, and materials for space applications. The syntheses are completed on a large scale according to current safety standards, using (up to) grams of $^{241}AmO_2$, various approaches such as sol-gel and direct co-precipitation. Representative examples are fuels for the SPHERE [87] and MARINE [88–91] irradiation experiments.

In the frame of demonstrating the potential use of ^{241}Am for space applications, a UKNNL-JRC cooperation began in 2015, focusing on the sinterability of Am_2O_3 and AmO_2 powders [92]. Thus, eight pellets of about 0.4 g each were produced and sintered, showing that formation of high-density pellets of AmO_2 *via* oxidation of Am_2O_3 sintered pellets is not a viable option.

In the past decade, approximately 15 g of americium were processed in the MALab, generating around 25 different compositions for the given purpose. Due to the rigorous use of manipulators and remote handling equipment, the effective radiation dose received by operators consistently remained well below the accepted limits. The operation was done with continuous support from the design office, workshop, analytical service, material transport, waste treatment and disposal, and radiation protection groups.

The pellets used for a microscale application of an americium source were produced using a gel-supported external hydrolysis method [22]. A mixed Am–U nitrate solution was dropped into an ammonia bath, resulting in a precipitate that was subsequently calcined. The calcination process involved heating for 2 h at 800 °C in air, followed by 6 h at the same temperature in an atmosphere of Ar/5 % H_2. After pressing, two main pellets (Fig. 5a) were sintered at 1600 °C in an atmosphere of $Ar/H_2/H_2O$ (2000 ppm). The first pellet (N1) had a height of 10.6 mm and a diameter of 6.0 mm. It had a mass of 2.96 g, which includes 2.13 g of ^{241}Am. The estimated thermal power generated by radioactive decay for this pellet was 243 mW_{th}. The second pellet (N2) was shaped like a disc, measuring 1.9 mm in height and 15.3 mm in diameter. Its mass was 3.33 g, which contained 2.41 g of ^{241}Am; the associated thermal heat power for this disc-shaped pellet was 271 mW_{th}. Both the pellet and the disc achieved a density of approximately 93 % of the theoretical density (TD) [22].

The mechanical stability of the pellet was assessed during seven years post-production. A visual inspection confirmed that the pellet and the disc maintained their integrity, showing no signs of pulverization or visible cracks in their macrostructure; Fig. 5*a* displays images of the pellet and the disc right after production and after seven years. In the initial years of study, the phenomenon of crystallographic swelling was monitored as well by XRD (Fig. 5b). Observations indicated that the crystallographic swelling of this material reached a maximum increase of approximately 0.4 % of the initial value in volume for about 0.1–0.2 dpa, representing circa half of the values reported for pure PuO_2/AmO_2. This minimal level of crystallographic swelling demonstrates the material's favourable performance under α self-irradiation, which is promising for its potential use as a heat source in space applications. Moreover, dimensional measurements do not show any macroscopic swelling over the error bar of the measurements.

5. Am-based RTG: microscale application

We present further a proof of concept, to demonstrate the feasibility of supplying energy to an equipment based on the heat produced by the above-described $Am_{1-y}U_yO_{2-x}$ pellets [22]. The total amount of heat power produced (514 mW_{th}) was relatively small, representing only a fraction of what is typically needed for standard mechanical devices including those that employ mechanical electricity conversion (such as micro-piezo pumps [93], micro-electric engines [94], and micro-thermodynamic engines like Stirling engines [95]). Therefore, the decision was made to generate electricity directly from the ^{241}Am source to power a real device. The operable set up had to fulfil several technical

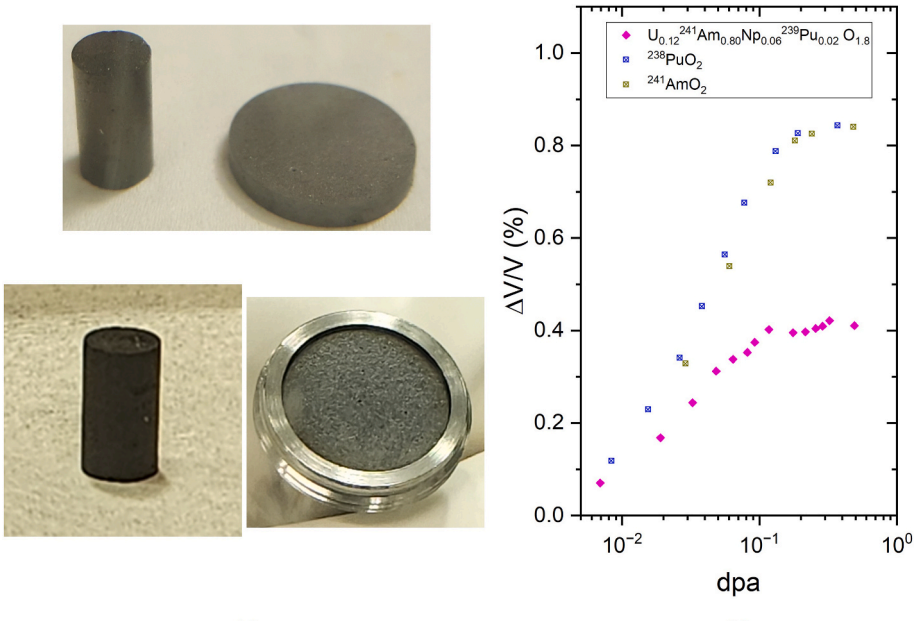

Fig. 5. (a) Images of the N1 pellet and N2 disc right after production (top) and after seven years (bottom) (b) Crystallographic swelling of the $Am_{1-y}U_yO_{2-x}$ pellet measured by XRD; the error bar on the y-axis (derived from Rietveld refinement) is withing the dimension of the symbols.

constraints.

(i) Regular and long term tested RTGs developed for electricity generation [96] are based on thermoelectricity conversion principle - Seebeck effect [97]. We know that typically only 5 % conversion of the thermal power is achievable and represents ~10 mW_e at best in our case.

(ii) It is not technically possible to simulate deep space conditions (temperature ~50–100 K at ultrahigh vacuum ~10^{-6} Pa) for a multiyear test. Nitrogen atmosphere of the glovebox and the circulation imposed by safety regulations, implied the presence of gas flow, increasing thermal heat transfer between hot and cold points on the pellet and reducing ΔT and Seebeck heat conversion. A conservative 1–2 mW_e available was taken for exploring technical solutions.

(iii) Simplified/robust technology as the components will be exposed to high radiation doses (^{241}Am). Moreover, only a few parameters need to be monitored, particularly temperature, ideally without electrical wiring, to showcase the fully autonomous nature of the setup. This requires wireless communication between the powered device and the receiver, using technologies such as Bluetooth or Wi-Fi.

From a survey of existing electronic components or systems (industry or research) requiring a minimal amount of power to function, we identified an industrial microelectronics equipment [98] that could be adapted/diverted from its design applications and could be powered by a fraction of ^{241}Am self-decay heat (~1 mW_e). The device is working on the concept of harvesting heat loss from warming radiators and is used for wireless monitoring and controlling temperatures in industrial buildings or individual homes [99]. Measured temperature values are transferred by Wi-Fi signal to a PC with reception antenna dedicated and supporting a monitoring software. All the information is gathered without wiring any probes to the central command and can be installed in the glove box with the pellet. The key interest, of course, is to get a fully autonomous setup (pellet + electronic device) reproducing at microscale ^{238}Pu-based RTG as in deep space probes [100] or on Mars missions [101].

To our best knowledge, the setup described (Fig. 6) is the first one ever reported operating completely autonomously on power generated by ^{241}Am isotope, the device being operated continuously at JRC-KA in the MALab since 2018. Temperatures (Cold and Hot) at the pellet contact and the heat sink, as well as the estimated electrical power generated by thermometric conversation, are reported in Fig. 7. It is important to emphasise that the demonstration presented here is not intended as a full-scale RTG prototype, but rather as the first experimental validation that an americium-based ceramic can power an autonomous electronic device over multi-year timescale. While the output remains at the milliwatt level and testing conditions differ from deep-space environments, this proof-of-concept provides a crucial step toward practical deployment. It demonstrates that americium ceramics, fabricated under remote-handling conditions, can maintain their integrity and functionality in a real, continuous operation.

6. Summary and outlook

This work discusses the outcome of a decade-long research effort focussed on producing stable americium-based ceramics, which have potential applications in radioisotope power sources. The long-term lifecycle expectations of such americium ceramics are directly tied to their resistance against α-decay damage and helium production. As shown in this work, U-stabilised AmO_2 retains crystallinity with minimal swelling even after seven years, while other compounds (*e.g.* $AmPO_4$, $AmAlO_3$) undergo amorphization. Our analysis demonstrates that U-stabilised AmO_2 offers both structural and chemical robustness to sustain the required multi-decade operational lifespan of RPSs.

Importantly, the aspects considered here – fabricability, radiation tolerance, stability under varying atmospheres – are crucial factors for the fuel form in RPSs. By identifying U-stabilised AmO_2 as a leading candidate, this work directly supports the development of americium

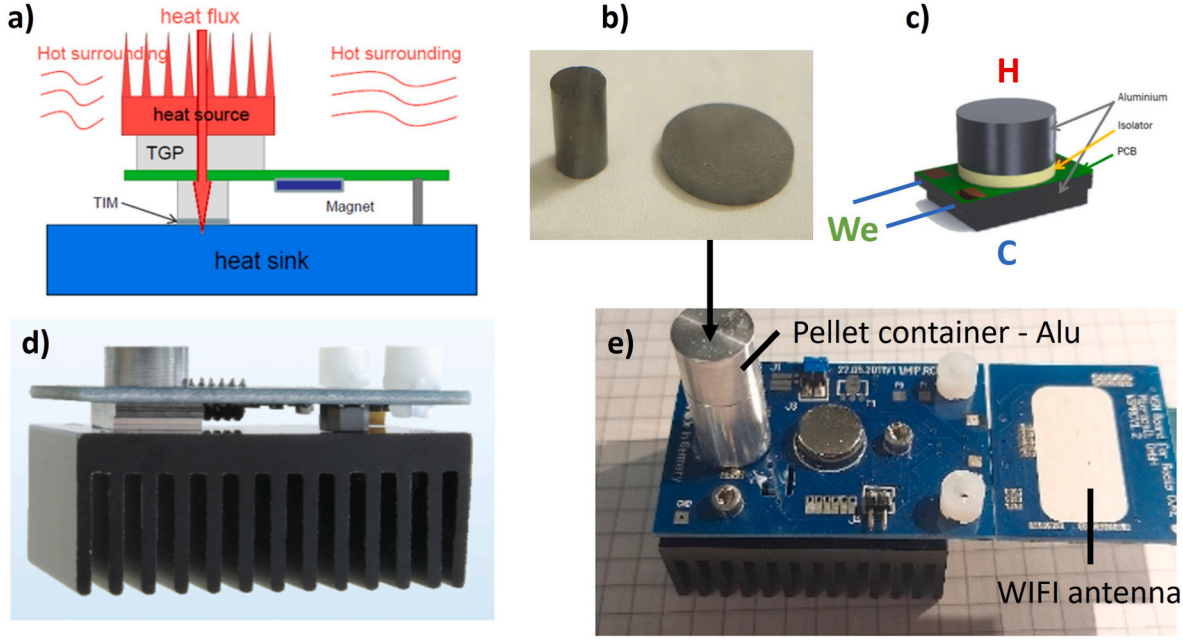

Fig. 6. (a) Principle of heat transfer in the setup and electrical power generated. The heat source (pellet/disk) should be in very good thermal contact with the Thermometric converter (ThermoGenerator in Package, TGP) shown in (c). In our case the heat sink is the black aluminium radiator in contact with atmosphere of the glove box. (b) Pellet/disc of $Am_{1-y}U_yO_{2-x}$ used for the experiment. (c) TGP converter with a diameter fitting with the section of the pellet. (H= Hot Side, C= Cold Side, We = electrical power generated by thermoelectric component powering temperature sensors (H and C) and Wi-Fi antenna (d) Unmodified device - MicroPelt © - rf core. (e) Set-up modified with aluminium block with the americium pellet inside and Wi-Fi antenna emitter in the glove box. Millimetre paper used for size reference.

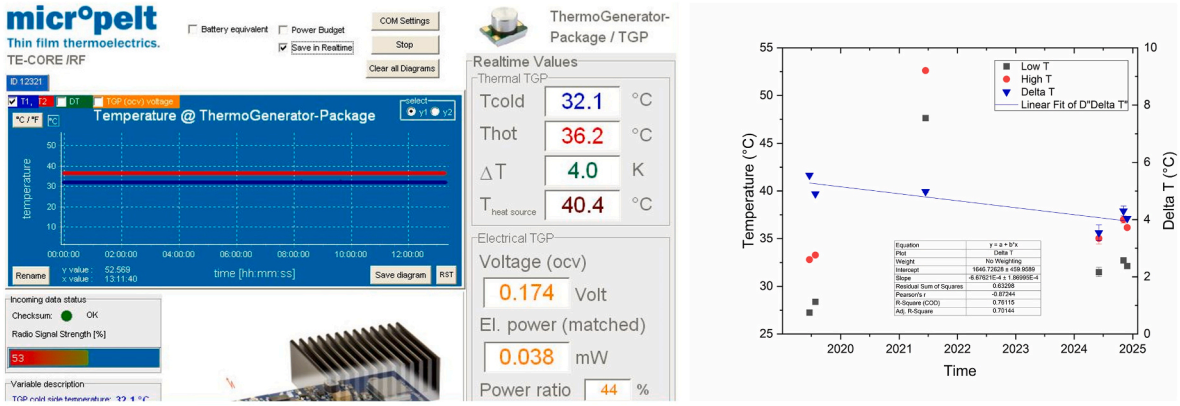

(a) (b)

Fig. 7. (a) Interface software with parameters monitored by the setup. (b) Temperatures recorded by the TE-CORE/RF from MicroPelt© on the $Am_{1-y}U_yO_{2-x}$ pellet/disc (fabrication: May 23, 2017); the total error in temperature reports is 1 °C (typical calibration error of the sensors is 0.5 °C and the measurements is also inducing ~0.5 °C error).

fuel forms for future RHU and RTG concepts of ESA, bridging the gap between isotope availability and system-level deployment. The next phase of this research should focus on upscaling of the fabrication process, including encapsulation, to produce batches ranging from tens to hundreds of grams, and optimising the microstructure of the ceramic source to facilitate helium release. This phase will likely focus on the realisation of the RHU design.

As described in some detail, the handling of ^{241}Am required for producing two $(Am,U)O_2$ pellets of about 3 g each was done by remote handling (JRC MALab). Our experience illustrates the complexity of working with this isotope at such a scale. The challenges for upscaling of source size will centre around proper management of radiation doses and heat production. This will require significant modifications compared to the current MALab design and operational practice, while maintaining source purity and quality, minimising handling losses. In particular, increase of automation/robotisation of the process will be necessary, and fabrication process and radioprotection approach must be brought in line with the feed material properties. The latter are currently not known, which effectively will delay the microstructure optimisation.

Finally, the development of a simple proof of concept demonstrated the feasibility of supplying electric energy to equipment with the stabilised AmO_2 pellets. The system has operated for more seven years, showing that it can generate completely autonomous electric current while maintaining the stability of the chosen material throughout this period. With upscaling of the source size, future tests can be more representative and investigate the effects of γ-radiation on the thermoelectric couples, an issue that is not occurring for ^{238}Pu sources.

CRediT authorship contribution statement

Jean-François Vigier: Writing – review & editing, Writing – original draft, Investigation, Data curation, Conceptualization. **Daniel Freis:** Writing – review & editing, Project administration, Conceptualization. **Rudy J.M. Konings:** Writing – review & editing, Writing – original draft, Resources, Project administration, Conceptualization. **Jérémie Manaud:** Writing – review & editing, Writing – original draft, Investigation, Data curation. **Philippe E. Raison:** Writing – review & editing, Writing – original draft, Investigation. **Patrick Lajarge:** Writing – review & editing, Investigation. **Sebastien Gardeur:** Writing – review & editing, Investigation. **Sorin Octavian Vălu:** Writing – review & editing, Investigation. **Jean-Christophe Griveau:** Writing – review & editing, Writing – original draft, Investigation, Data curation, Conceptualization. **Karin Popa:** Writing – review & editing, Writing – original draft, Project administration, Investigation, Conceptualization.

Declaration of generative AI and AI-assisted technologies in the writing process

No generative AI and AI-assisted technologies were used for writing the present paper.

Declaration of competing interest

The authors declare that they have no known competing financial interests or personal relationships that could have appeared to influence the work reported in this paper.

Acknowledgements

We would like to thank Christian Berkmann, Jacobus Boshoven, Daniel Bouëxière, Andrea Cambriani, Antony Guiot, Herwin Hein, Michael Holzhäuser, Sven Pfirrmann, Alfred Rothermel and Chris Selfslag, who provided exceptional technical assistance in the design and practical conduct of the experiments to which this paper referred.

Data availability

No data was used for the research described in the article.

References

[1] J.M. Davis, R.L. Cataldo, J.F. Soeder, M.A. Manzo, R. Hakimzadeh, An overview of power capability requirements for exploration missions, NASA Center for Aerospace Information, Hanover (2005).
[2] W. Wu, J. Shen, H. Kong, Y. Yang, E. Ren, Z. Liu, W. Wang, M. Dong, L. Han, C. Yang, H. Zheng, Q. Xu, X. Yao, J. Zhao, S. Li, Q. Yang, J. Liu, Y. Zhang, J. Li, Y. Guo, J. Li, M. Li, H. Liu, D. Zheng, R. Xiong, J. Ma, D. Zhang, Energy system and resource utilization in space: a state-of-the-art review, The Innovation Energy 1 (2) (2024).
[3] M. Prelas, M. Boraas, F. De La Torre Aguilar, J.D. Seelig, M. Tchakoua Tchouaso, D. Wisniewski, Potential applications for nuclear batteries, in: Nuclear Batteries and Radioisotopes 56, Springer, 2016, pp. 265–305. Lecture Notes in Energy.
[4] J.S. Dustin, R.A. Borrelli, Assessment of alternative radionuclides for use in a radioisotope thermoelectric generator, Nucl. Eng. Des. 385 (2021) 111475.
[5] D. Champier, Thermoelectric generators: a review of applications, Energy Convers. Manag. 140 (2011) 167–181.
[6] S. Yang, H. Chen, D. Luo, A comprehensive review of thermoelectric generators from micropower supply to kilowatt system, Green Energy and Fuel Research 2 (2) (2025) 93–108.
[7] D. Kramer, Shortage of plutonium-238 jeopardizes NASA's planetary science missions, Phys. Today 64 (1) (2011) 24–26.
[8] C. Campbell, C. Carrigan, M. Carrot, C. Maher, B. McLuckie, C. Mason, C. Gregson, T.H.J. Griffiths, M. Sarsfield, R. Taylor, T. Tinsley, K. Stephenson, The separation of 241Am from aged plutonium dioxide for use in radioisotope power systems using the AMPPEX process, Procedia Chem. 21 (2016) 140–147.

[9] R.M. Ambrosi, H. Williams, E.J. Watkinson, A. Barco, R. Mesalam, T. Crawfort, C. Bicknell, P. Samara-Ratna, D. Vernon, N. Bannister, D. Ross, J. Sykes, M.-C. Perkinson, C. Burgess, C. Stroud, S. Gibson, A. Godfrey, M. Reece, European Radioisotope Thermoelectric Generators (RTGs) and Radioisotope Heater Units (RHUs) for space science and exploration, Space Sci. Rev. 215 (55) (2019) 1–41.

[10] S. Bourgh, T. Matsumura, A. Khaperskaia, S. Palethorpe, R. Taylor, E. Collins, B. Delcul, J. Law, G. Lumetta, P. Soucek, S. Cornet, G. Grassi, Unlocking the Hidden Value of Nuclear Fuel: the Societal Benefits of Diverse Material Recycling, OECD Nuclear Energy Agency, NEA, 2024.

[11] Orano White papers [Online]. Available: https://www.orano.group/usa/en/our-portfolio-expertise/orano-white-papers/potential-radioisotope-element-harvesting-from-recycling-of-unf.

[12] R. Mesalam, P.C. Schmitz, H.M. Sargeant, E.R. Turnbull, A. Barco, S. Wilson, J. Stuck, E.J. Watkinson, S.R. Oleson, R. Ambrosi, Americium fuelled radioisotope stirling generator for lunar surface mobility systems, Acta Astronaut. 228 (2025) 331–345.

[13] J. Brown, C. Campbell, C. Carrigan, M. Carrott, K. Greenough, C. Maher, B. McLuckie, C. Mason, C. Gregson, T. Griffiths, J. Holt, M. Sarsfield, K. Stephenson, R. Taylor, T. Tinsley, Americium and plutonium purification by extraction (the AMPPEX process): development of a new method to separate 241Am from aged plutonium dioxide for use in space power systems, Prog. Nucl. Energy 106 (2018) 396–416.

[14] P. Benetti, A. Cesena, L. Cinotti, L.T.M. Raselli, Americium 242m and its potential use in space applications, J. Phys. Conf. 41 (2006) 161–168.

[15] W.W. Schultz, The Chemistry of Americium, Energy Research and Development Administration, 1976. Technical Information Center.

[16] K. Li, C. Yan, J. Wang, K. Zhu, J. Guo, Y. Zhang, G. Shi, Y. Yin, L. Cheng, L. Sun, Y. Wang, H. Zhang, Y. Sun, J. Yuan, W. Ma, G. Ji, Z. Chai, Y. Wang, X. Ouyang, S. Wang, Micronuclear battery based on a coalescent energy transducer, Nature (2024) 811–815.

[17] E. Gibney, How nuclear waste will help spacecraft explore the Moon - and beyond, Nature 612 (2022) 385–386.

[18] D. Freis, J.-F. Vigier, K. Popa, R.J.M. Konings, Research in support of European Radioisotope power system development at the European commission's joint research centre in Karlsruhe, ATW - Int. J. Nucl. Power 65 (4) (2020) 198–205.

[19] E.F. Westrum, L. Eyring, The preparation and some properties of americium metal, J. Am. Chem. Soc. 73 (7) (1951) 3396–3398. Jr.

[20] T.D. Chikalla, L. Eyring, Phase relationships in the americium oxygen system, J. Inorg. Nucl. Chem. 30 (1) (1968) 133–145.

[21] E. Epifano, C. Guéneau, R.C. Belin, R. Vauchy, F. Lebreton, J.-C. Richaud, A. Joly, C. Valot, P.M. Martin, Insight into the Am-O phase equilibria: a thermodynamic study coupling high-temperature XRD and CALPHAD modeling, Inorg. Chem. 53 (13) (2017) 7416–7432.

[22] J.-F. Vigier, D. Freis, P. Pöml, D. Prieur, P. Lajarge, S. Gardeur, A. Guiot, D. Bouëxière, R.J.M. Konings, Optimisation of uranium-doped americium oxide synthesis for space applications, Inorg. Chem. 57 (8) (2018) 4317–4327.

[23] M.T. Swinhoe, N. Ensslin, The origin of neutron radiation, in: Nondestructive Assay of Nuclear Materials for Safeguards and Security, Springer, 2024, pp. 289–306.

[24] M.T. Pigni, I.C. Gauld, S. Croft, (α,n) reactions in oxide compounds calculated from the R-matrix theory, Prog. Nucl. Energy 118 (2020) 103130:1–8.

[25] ICSD, Inorganic crystal structure database [Online]. Available: https://icsd.fiz-karlsruhe.de/, 2024.

[26] W.H. Runde, W.W. Schulz, Americium, in: The Chemistry of the Actinide and Transactinide Elements, Springer, Dordrecht, 2010, pp. 1265–1395.

[27] T.K. Deason, H.B. Tisdale, A.T. Hines, G. Morrison, Y. Zhoujin, M.D. Smith, T. M. Besmann, A.M. Mofrad, S.L. Estes, J.W. Amoroso, D.P. DiPrete, H.-C. zur Loye, Investigation of americium-containing phosphates, silicates, borates, molybdates, and fluorides synthesized via high-temperature flux crystal growth, J. Am. Chem. Soc. 147 (25) (2025) 21659–21671.

[28] K. Popa, J.-F. Vigier, L. Martel, D. Manara, J.-Y. Colle, O. Dieste Blanco, T. Wiss, D. Freis, R.J.M. Konings, Synthesis, characterization, and stability of americium phosphate, AmPO4, Inorg. Chem. 59 (9) (2020) 6595–6602.

[29] J.-F. Vigier, T. Wiss, N. Palina, T. Vitova, J.-Y. Colle, D. Bouëxière, D. Freis, R.J. M. Konings, K. Popa, Synthesis, characterization, and stability of two americium vanadates, AmVO3 and AmVO4, Inorg. Chem. 62 (24) (2023) 9350–9359.

[30] J.-F. Vigier, K. Popa, L. Martel, D. Manara, O. Dieste Blanco, D. Freis, R.J. M. Konings, Plutonium and americium aluminate perovskites, Inorg. Chem. 58 (14) (2019) 9118–9126.

[31] B. Schacherl, M. Tagliavini, H. Kaufmann-Heimeshoff, J. Göttlicher, M. Mazzanti, K. Popa, O. Walter, T. Pruessmann, C. Vollmer, A. Beck, R.S.K. Ekanayake, J. A. Branson, T. Neill, D. Fellhauer, C. Reitz, D. Schild, D. Brager, T. Vitova, Resonant inelastic X-ray scattering tools to count 5 f electrons of actinides and probe bond covalency, Nat. Commun. 16 (2025) 1–21.

[32] U. Benedict, C. Dufour, Low temperature lattice expansion of americium dioxide, Physica B+C 102 (1–3) (1980) 303–307.

[33] E. Epifano, M. Naji, D. Manara, A.C. Scheinost, C. Hennig, J. Lechelle, R.J. M. Konings, C. Guéneau, D. Prieur, T. Vitova, K. Dardenne, J. Rothe, P.M. Martin, Extreme multi-valence states in mixed actinide oxides, Commun. Chem. 2 (59) (2019) 1–11.

[34] E. Epifano, R. Vauchy, F. Lebreton, A. Joly, C. Guéneau, C. Valot, P.M. Martin, Behaviour of (U,Am)O2 in oxidizing conditions: a high-temperature XRD study, J. Nucl. Mater. 531 (2020) 1–11.

[35] F. Lebreton, D. Horlait, T. Delahaye, P. Blanchart, Fabrication and characterization of U1−xAmxO2±δ compounds with high americium contents (x=0.3, 0.4 and 0.5), J. Nucl. Mater. 439 (1–3) (2013) 99–102.

[36] E. Epifano, R. Vauchy, F. Lebreton, R. Lauwerier, A. Joly, A. Scheinost, C. Guéneau, C. Valot, P.M. Martin, On the O-rich domain of the U-Am-O phase diagram, J. Nucl. Mater. 531 (2020) 1–10.

[37] R. Vauchy, S. Hirooka, M. Watanabe, K. Yokoyama, T. Murakami, Lattice parameters of fluorite-structured uranium-americium mixed oxides, J. Nucl. Mater. 584 (2023) 1–12.

[38] J.-F. Vigier, D. Freis, O. Walter, O. Dieste Blanco, D. Bouëxière, E. Zuleger, N. Palina, T. Vitova, R.J.M. Konings, K. Popa, Synthesis and characterization of homogeneous (U,Am)O2 and (U,Pu,Am)O2 nanopowders, CrystEngComm 24 (2022) 6338–6348.

[39] B.C. Chakoumakos, Systematics of the pyrochlore structure type, ideal A2B2X6Y, J. Solid State Chem. 53 (1) (1984) 120–129.

[40] P.E. Raison, R.G. Haire, T. Sato, T. Ogawa, Fundamental and technological aspects of actinide oxide pyrochlores: relevance for immobilization matrices, MRS Online Proc. Libr. 556 (1998) 3–10.

[41] R.G. Haire, P.E. Raison, Z. Assefa, Systematic studies of the fundamental chemistry of pyrochlore oxides: An2Zr2O7 [An = Pu, Am, Cm, Bk and Cf], J. Nucl. Sci. Technol. 39 (sup3) (2002) 616–619.

[42] M.A. Subramanian, G. Aravamudan, G.V. Subba Rao, Oxide pyrochlores - a review, J. Solid State Chem. 15 (2) (1983) 55–143.

[43] R.C. Belin, P.J. Valenza, P.E. Raison, Structure of the americium pyrochlore Am2Zr2O7 and its evolution under alpha self-irradiation, in: Recent Advances in Actinide Science, The Royal Society of Chemistry, Cambridge, 2006, pp. 352–354.

[44] R.C. Belin, P.J. Valenza, P.E. Raison, M. Tillard, Synthesis and rietveld structure refinement of americium pyrochlore Am2Zr2O7, J. Alloys Compd. 448 (1–2) (2008) 321–324.

[45] A.F. Fuentes, S.M. Montemayor, M. Maczka, M. Lang, R.C. Ewing, U. Amador, A critical review of existing criteria for the prediction of pyrochlore formation and stability, Inorg. Chem. 57 (19) (2018) 12093–12105.

[46] D. Prieur, J.-F. Vigier, T. Wiss, A. Janssen, J. Rothe, A. Cambriani, J. Somers, Structural investigation of self-irradiation damaged AmO2, J. Nucl. Mater. 212 (2014) 7–12.

[47] D. Horlait, F. Lebreton, P. Roussel, T. Delahaye, XRD monitoring of α self-irradiation in uranium–americium mixed oxides, Inorg. Chem. 52 (24) (2013) 14196–14204.

[48] R.C. Belin, P.M. Martin, P.J. Valenza, A.C. Scheinost, Experimental insight into the radiation resistance of zirconia-based americium ceramics, Inorg. Chem. 48 (12) (2009) 5376–5381.

[49] F. Goubard, P. Griesmar, A. Tabuteau, Alpha self-irradiation effects in ternary oxides of actinide elements: the zircon-like phases AmIIIVO4 and AIINpIV(VO4)2 (A = Sr, Pb), J. Solid State Chem. 178 (2005) 1898–1902.

[50] A.M. Seydoux-Guillaume, R. Wirth, J. Ingrin, Contrasting response of ThSiO4 and monazite to natural irradiation, Eur. J. Mineral 19 (1) (2007) 7–14.

[51] S. Neumeier, P. Kegler, Y. Arinicheva, A. Shelyug, P.M. Kowalski, C. Schreinemachers, A. Navrotsky, D. Bosbach, Thermochemistry of La1-xLnxPO4-monazites (Ln= Gd, Eu), J. Chem. Therm. 105 (2017) 396–403.

[52] C.M. Gramaccioli, T.V. Segalstad, A uranium- and thorium-rich monazite from a South-Alpine pegmatite at Piona, Italy, Am. Mineral. 63 (7–8) (1978) 757–761.

[53] B.E. Burakov, M.A. Yagovkina, V.M. Garbuzov, A.A. Kitsay, V.A. Zirlin, Self-Irradiation of Monazite Ceramics: Contrasting Behavior of PuPO4 and (La,Pu)Po4 Doped with Pu-238, 824, MRS Online Proceedings Library (OPL), 2004.

[54] K. Popa, P.E. Raison, L. Martel, P.M. Martin, D. Prieur, P.L. Solari, D. Bouëxière, R.J.M. Konings, J. Somers, Structural investigations of Pu(III) phosphate by X-ray diffraction, MASNMR and XANES spectroscopy, J. Solid State Chem. 230 (2015) 169–174.

[55] Y. Arinicheva, K. Popa, A. Scheinost, A. Rossberg, O. Dieste-Blanco, P.E. Raison, A. Cambriani, J. Somers, D. Bosbach, S. Neumeier, Structural investigations of (La,Pu)PO4 monazite solid solutions: XRD and XAFS study, J. Nucl. Mater. 493 (2017) 404–411.

[56] L. Martel, M. Ashraful Islam, K. Popa, J.-F. Vigier, E. Colineau, H. Bolvin, J.-C. Griveau, Local structure and magnetism of La1-xMxPO4 (M = Sm, 239Pu, 241Am) explained by experimental and computational analyses, J. Phys. Chem. C 125 (40) (2021) 22163–22174.

[57] R.C. Ewing, W.J. Weber, Actinide waste forms and radiation effects, in: The Chemistry of the Actinide and Transactinide Elements, Springer, Netherlands, 2010, pp. 3813–3887.

[58] L. Nasdala, M. Wenzel, G. Vavra, G. Irmer, T. Wenzel, B. Kober, Metamictisation of natural zircon: accumulation versus thermal annealing of radioactivity-induced damage, Contrib. Mineral. Petrol. 141 (2) (2001) 125–144.

[59] W.J. Weber, R.C. Ewing, L.M. Wang, The radiation-induced crystalline-to-amorphous transition in zircon, J. Mater. Res. 9 (3) (1994) 688–698.

[60] V.A. Kudryavtsev, P. Zakhary, B. Easeman, Neutron production in (α,n) reactions, Nucl. Instrum. Methods Phys. Res. Sect. A Accel. Spectrom. Detect. Assoc. Equip. 972 (2020) 1–7.

[61] G.R. Lumpkin, A.N. Mariano, Natural occurrence and stability of pyrochlore in carbonatites, related hydrothermal systems, and weathering environments, MRS Online Proc. Libr. 412 (1995) 831–838.

[62] R.E. Sykora, P.E. Raison, R.G. Haire, Self-irradiation induced structural changes in the transplutonium pyrochlores An2Zr2O7 (An=Am, Cf), J. Solid State Chem. 178 (2) (2005) 578–583.

[63] S.V. Stefanovsky, A.G. Ptashkin, S.V. Yudintsev, B.F. Myasoedov, Alpha-decay effects in 241Am-doped gadolinium zirconate, MRS Online Proc. Libr. 1444 (2012) 237–242.

[64] P.M. Martin, R.C. Belin, P.J. Valenza, A.C. Scheinost, EXAFS study of the structural phase transition in the americium zirconate pyrochlore, J. Nucl. Mater. 385 (1) (2009).

[65] H. Otobe, M. Takano, H. Hayashi, Y. Arai, Oxygen potentials of pyrochlore-type Am2Zr2O7+y, J. Am. Chem. Soc. 94 (10) (2011) 3596–3599.
[66] L. Ramond, P.P.S. Coste, A. Gauthé, M. Bataillea, Fabrication of (U,Am)O2 pellet with controlled porosity from oxide microspheres, J. Nucl. Mater. 492 (2017) 97–101.
[67] J.W. Boyce, K.V. Hodges, W.J. Olszewski, M.J. Jercinovic, He diffusion in monazite: implications for (U-Th)/He thermochronometry, Geochem. Cosmochim. Acta 71 (16) (2005) 4015–4024.
[68] D.J. Cherniak, Diffusion in accessory minerals: Zircon, titanite, apatite, monazite and xenotime, Rev. Mineral. Geochem. 72 (1) (2010) 827–869.
[69] D.J. Cherniak, E.B. Watson, Diffusion of helium in natural monazite, and preliminary results on He diffusion in synthetic light rare earth phosphates, Am. Mineral. 98 (8–9) (2013) 1407–1420.
[70] K.A. Farley, He diffusion systematics in minerals: evidence from synthetic monazite and zircon structure phosphates, Geochem. Cosmochim. Acta 71 (16) (2007) 4015–4024.
[71] C.A. Taylor, M.K. Patel, J.A. Aguiar, Y. Zhang, M.L. Crespillo, J. Wen, H. Xue, Y. Wang, Bubble formation and lattice parameter changes resulting from He irradiation of defect-fluorite Gd2Zr2O7, Acta Mater. 115 (2016) 115–122.
[72] D.E. Peterson, J.W. Early, J.S. Starzynski, C.C. Land, Helium Release from Radioisotopic Heat Sources, Los Alamos National Laboratory, 1984.
[73] W.D. Neilson, H. Steele, N. Kaltsoyannis, S.T. Murphy, Accommodation of helium in PuO2±x and the role of americium, Phys. Chem. Chem. Phys. 24 (14) (2022) 8245–8250.
[74] T. Wiss, R.J.M. Konings, D. Staicu, A. Benedetti, J.-Y. Colle, V.V. Rondinella, E. Maugeri, Z. Talip, A. Janssen, O. Dieste, L. Cognini, E. De Bona, G. Baldinozzi, C. Guéneau, Impact of alpha-damage and helium production on the heat capacity of actinide oxides, Front. Nucl. Eng. 4 (2025) 1–20.
[75] R.A. Brockman, D.P. Kramer, C.D. Barklay, D. Cairns-Gallimore, J.L. Brown, J. C. Huling, C.E. Van Pelt, Modeling of selected ceramic processing parameters employed in the fabrication of 238PuO2 fuel pellets, Phys. Procedia 20 (2011) 397–403.
[76] E.J. Watkinson, R. Mesalam, J.-F. Vigier, O. Beneš, J.-C. Griveau, E. Colineau, M. Sierig, D. Freis, R.M. Ambrosi, D.K.R.J.M. Staicu, Thermal properties and behaviour of Am-bearing fuel in European Space radioisotope power systems, Thermoelectrics 1 (3) (2021) 297–331.
[77] D. Staicu, T. Wiss, V.V. Rondinella, P.-J. Hiernaut, R.J.M. Konings, C. Ronchi, Impact of auto-irradiation on the thermophysical properties of oxide nuclear reactor fuels, J. Nucl. Mater. 397 (1–3) (2020) 8–18.
[78] S.O. Vălu, O. Beneš, E. Colineau, J.-C. Griveau, R.J.M. Konings, The low-temperature heat capacity of (U1-yAmy)O 2−x for y = 0.08 and 0.20, J. Nucl. Mater. 507 (2018) 126–134.
[79] S.O. Vălu, E. De Bona, K. Popa, J.-C. Griveau, E. Colineau, R.J.M. Konings, The effect of lattice disorder on the low-temperature heat capacity of (U1-yThy)O2 and 238Pu-doped UO2, Sci. Rep. 9 (2019) 1–10.
[80] J.-C. Griveau, J.-F. Vigier, K. Popa, S.-O. Vălu, E. Colineau, R.J.M. Konings, Low-temperature heat capacity and magnetism in (U1−yLny)O2 and (U1−yAmy)O2 (y = 0.01 − 0.05) solid solutions: effects of substitution and self-irradiation, J. Appl. Phys. 132 (2022) 1–13.
[81] S. Lutique, R.J.M. Konings, V.V. Rondinella, J. Somers, T. Wiss, The thermal conductivity of Nd2Zr2O7 pyrochlore and the thermal behaviour of pyrochlore-based inert matrix fuel, J. Alloys Compd. 352 (1–2) (2003) 1–5.
[82] T. Nishi, M. Takano, A. Itoh, M. Akabori, Y. Arai, K. Minato, M. Numata, Thermal conductivity of AmO2-x, J. Nucl. Mater. 373 (1–3) (2008) 295–298.
[83] S. Chong, B.J. Riley, X. Lu, J. Ju, T. Mahadevan, V. Hegde, Synthesis and properties of anhydrous rare-earth phosphates, monazite and xenotime: a review, RSC Adv. 14 (27) (2024) 18978–19000.
[84] F. Nakamori, Y. Ohishi, M. H, K. Kurosaki, K.i. Fukumoto, S. Yamanaka, Mechanical and thermal properties of ZrSiO4, J. Nucl. Sci. Technol. 54 (11) (2017) 1267–1273.
[85] R. Guo, Thermophysical Properties and Radiation Damage of NdCrO3 and NdAlO3, UNSW Library, 2016.
[86] European Parliament, Euratom treaty [Online]. Available: https://www.europarl.europa.eu/about-parliament/en/in-the-past/the-parliament-and-the-treaties/euratom-treaty, 25 March 1957.
[87] E. D'Agata, P.R. Hania, J. McGinley, J. Somers, C. Sciolla, P.J. Baas, S. Kamer, R. A.F. Okel, I. Bobeldijk, F. Delage, S. Bejaoui, SPHERE: irradiation of sphere-pac fuel of UPuO2−x containing, Nucl. Eng. Des. (2014) 300–311.
[88] E. D'Agata, P.R. Hania, D. Freis, J. Somers, S. Bejaoui, F.F. Charpin, P.J. Baas, R. A.F. Okel, S. van Til, J.-M. Lapetite, F. Delage, The MARINE experiment: irradiation of sphere-pac fuel and pellets of UO2-x for americium breading blanket concept, Nucl. Eng. Des. (2017) 131–141.
[89] S. van Til, P.R. Hania, A.V. Fedorov, E. D'Agata, D. Freis, S. Bejaoui, F. Delage, A. Gallais-During, Irradiation performance and first examinations of Americium bearing blanket fuel from the MARINE irradiation experiment, J. Nucl. Mater. (2023) 154699.
[90] A. Fernandez, K. Richter, J. Somers, Fabrication of transmutation and incineration targets by infiltration of porous pellets by radioactive solutions, J. Alloys Compd. 271–273 (1998) 616–619. Vols.
[91] M. Vespa, M. Rini, J. Spino, T. Vitova, J. Somers, Fabrication and characterization of (U, Am)O2−x transmutation targets, J. Nucl. Mater. 421 (1–3) (2012) 80–88.
[92] M.J. Sarsfield, C. Campbell, C.C.M.J. Carrigan, J.-Y. Colle, D. Freis, C. Gregson, T. Griffiths, J. Holt, P. Lajarge, C.J. Maher, D. Manara, B. McLuckie, C. Mason, M. Naji, R.J. Taylor, T. Tisley, J. Somers, J.-F. Vigier, The separation of 241Am from aged plutonium dioxide for use in radioisotope power systems, E3S Web of Conferences 16 (2017) 1–8.
[93] Piezoelectric micro pump - cartridge type [Online]. Available: https://www.takasago-fluidics.com/products/sdmp-c.
[94] J.H. Cho, L.W. Weiss, C.D. Richards, D.F. Bahr, R.F. Richards, Power production by a dynamic micro heat engine with an integrated thermal switch, J. Micromech. Microeng. 17 (9) (2007) S217.
[95] W.-L. Chen, G.M.D. Currao, C.-Y. Wu, B.-Y. Thai, S.-C. Lin, C.-J. Li, An experimental analysis on a stirling-engine-driven micro power-generation system integrated with a flat-flame burner powered by dimethyl ether fuel mixed with ammonia, Energy 314 (2025) 1–16.
[96] T. Li, Y. Liu, Y. Zhang, H. Chen, Q. Xiang, Comprehensive modeling and characterization of the general-purpose heat source radioisotope thermoelectric generator for solar system missions, Appl. Therm. Eng. B 248 (2024) 1–14.
[97] X. Zhu, Y. Yu, F. Li, A review on thermoelectric energy harvesting from asphalt pavement: configuration, performance and future, Constr. Build. Mater. 228 (2019) 1–13.
[98] MLRTPS LoRaWAN-Wallmount theromostat [Online]. Available: https://www.micropelt.com/.
[99] LoRaWAN-MLR003 LoraWAN heating solution [Online]. Available: https://www.micropelt.com/en/products/heating-cost-reduction.
[100] M.R. Swartz, Comparison of NANOR-type LANR Components to 238Pu as heat source for space flight, J. Condensed Matter Nucl. Sci. 29 (2019) 238–248.
[101] J. Urban-Klaehn, D. Miller, B.J. Gross, C.R. Tyler, C.C. Dwight, Initial phase of Pu-238 production in Idaho national laboratory, Appl. Radiat. Isot. 169 (2021) 1–8.